Synthesis and Spectroscopic Characterization of 1,8-Naphthalimide Derived "Super" Photoacids

Kumpulainen, T.; Bakker, B.H.; Hilbers, M.; Brouwer, A.M.

DOI
10.1021/jp508334s

Publication date
2015

Document Version
Final published version

Published in
The journal of Physical Chemistry. B

THE JOURNAL OF PHYSICAL CHEMISTRY B

Article

pubs.acs.org/JPCB

Synthesis and Spectroscopic Characterization of 1,8-Naphthalimide Derived "Super" Photoacids

Tatu Kumpulainen, Bert H. Bakker, Michiel Hilbers, and Albert M. Brouwer*

Van 't Hoff Institute for Molecular Sciences, Faculty of Science, University of Amsterdam, P.O. Box 94157, 1090 GD Amsterdam, The Netherlands

Supporting Information

ABSTRACT: The ground- and excited-state acid–base properties of three novel naphthalimide-based "super" photoacids were studied using steady-state and time-resolved spectroscopy. The compounds exhibit pK_a = 8.8–8.0 and pK_a^* = −1.2 to −1.9. The decrease in both ground- and excited-state pK_a is achieved by attachment of an electron withdrawing group (sulfonate) on the aromatic system. All compounds are deprotonated upon excitation in alcohols and DMSO. Good correlation is established between the pK_a^* and the ratio of the neutral and anion emission intensities in a certain solvent. The excited-state intermolecular proton transfer to solvent (H_2O and DMSO) is explained by a two-step model. In the first step, short-range proton transfer takes place, resulting in the formation of a contact ion pair. Free ion pairs are formed in the diffusion controlled second step.

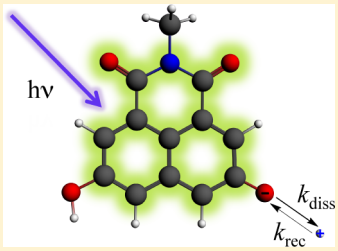

INTRODUCTION

The acidity of many hydroxy-substituted aromatic compounds increases dramatically upon electronic excitation. Excitation of a neutral form of this class of molecules, known as photoacids, results in excited-state proton transfer (ESPT) to the solvent in aqueous solutions. This is manifested by dual emission from the neutral (ROH*) and anionic (RO^-*) forms. After 60 years of its first description by Förster,[1] excited-state proton-transfer (ESPT) reactions remain an active topic in biology and physical chemistry[2−5] and the field has been reviewed several times.[6−10]

Most well-known classes of photoacids are based on naphthols,[11,12] hydroxyquinolines,[13,14] and hydroxypyrenes.[15,16] The photoacidity is generally explained by a partial intramolecular charge transfer from the hydroxyl oxygen to the aromatic ring in the excited state.[17−20] Thus, introduction of electron withdrawing groups, such as cyano or sulfonate groups, on the aromatic system increases the acidity in both the ground and excited states.

While 2-naphthol has a pK_a of 9.5 in the ground state and pK_a^* of 2.8 in the excited state, its cyano-functionalized derivatives exhibit $\Delta pK_a \approx -8$ to −12 units upon excitation and $pK_a^* \approx 0$ to −4 depending on the number and positions of the cyano groups. Tolbert et al. introduced the term "super" photoacids to describe these enhanced photoacids possessing negative pK_a^* values and the ability to deprotonate in organic solvents, such as alcohols and dimethyl sulfoxide (DMSO), in the absence of water.[12,21] Recently, Jung et al.[16] used a similar approach to enhance the acidity of the well-known 8-hydroxypyrene-1,3,6-trisulfonate (**HPTS**, $pK_a \approx 7.4$ and $pK_a^* \approx 0.4$)[22] photoacid. Substitution of the sulfonate groups by more electron withdrawing sulfonamide or sulfonic ester groups resulted in pK_a = 5.7–4.4 and pK_a^* = −0.8 to −3.9.

Substituted 1,8-naphthalimides are widely employed as probes and sensors due to their fluorescent properties.[23−25] The naphthalimide (**NI**) skeleton offers a flexible and robust template in which both aromatic and *N*-substitution are easily accessible.[26−28] Hydroxy-substitution of the aromatic system has been shown to introduce photoacidic properties resulting in dual fluorescence. Biczók et al. studied fluorescence quenching and intermolecular ion pair formation of 3- and 4-hydroxy-*N*-methyl-1,8-naphthalimides, but the studies were done solely in organic solvents.[29−31] To the best of our knowledge, no studies on excited-state acid–base reactions of hydroxy-1,8-naphthalimides in aqueous solutions have yet been reported.

We present now the syntheses and photophysical characterizations of three novel **NI**-derived photoacids (Scheme 1). First, we will report steady-state characterization of all three compounds in water and organic solvents. Second, we will show ps time-resolved fluorescence (time-correlated single photon counting, TCSPC) studies of all compounds in DMSO. Third, we will report a more thorough investigation of a selected photoacid, **EG-dHONI**, in aqueous solutions including ps time-resolved fluorescence and ns transient absorption (flash photolysis). We will also evaluate the possibility of dianion formation (deprotonation of both hydroxyl groups) by means of steady-state electronic and NMR spectroscopies. Last, we will show results of quantum chemical calculations (DFT and TD-DFT) to gain more insight into the effect of substitution on the photoacidic and spectroscopic properties.

The results are analyzed within the already established framework of ground- and excited-state acid–base reactions. Briefly, the overall deprotonation process will be explained by a

Special Issue: Photoinduced Proton Transfer in Chemistry and Biology Symposium

Received: August 18, 2014
Revised: September 15, 2014
Published: September 16, 2014

   dx.doi.org/10.1021/jp508334s | *J. Phys. Chem. B* 2015, 119, 2515–2524

Scheme 1. Synthetic Procedures of All Target Compounds[a]

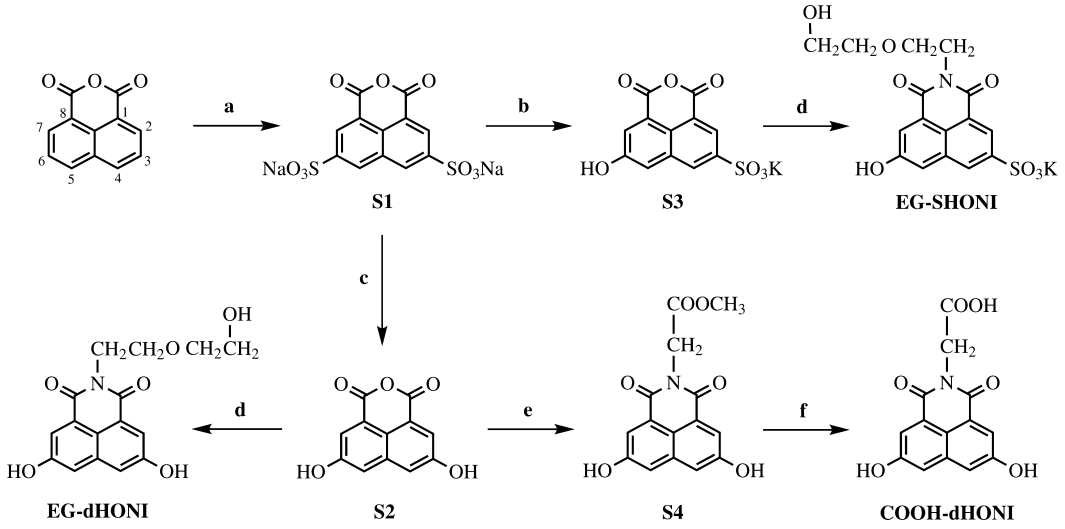

[a]Reaction conditions: (**a**) H_2SO_4/SO_3, 210 °C, 3 h; (**b**) KOH, 230 °C, 10 min; (**c**) KOH, 250 °C, 15 min; (**d**) $H_2NCH_2CH_2OCH_2CH_2OH$, ethanol, reflux, 20 h; (**e**) $H_2NCH_2COOCH_3$, ethanol, reflux, 20 h; (**f**) NaOH, ethanol/water (1/1), reflux, 1 h.

Scheme 2. Photophysical Scheme for the Two-Step Deprotonation Process[a]

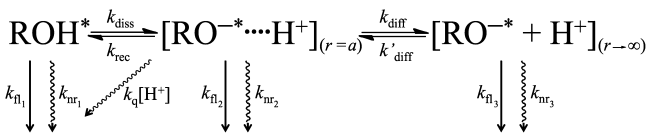

[a]Initial deprotonation results in the formation of the contact ion pair ($r = a$) followed by diffusion controlled formation of the free ions ($r \rightarrow \infty$).

two-step model (Scheme 2) originally proposed by Eigen and Weller.[6,32] In the model, the initial short-range proton transfer results in formation of a contact ion pair followed by diffusion controlled separation of the ions.[15,33,34] Different decay pathways are also indicated in the scheme including a quenching process by protons. The decay of the ground-state anion, measured by flash photolysis, is analyzed using pseudo-first-order, mixture of first- and second-order, and pure second-order reaction kinetics at low, intermediate, and neutral pH, respectively.[35,36]

EXPERIMENTAL SECTION

Materials. The reaction scheme for the synthesis of the target compounds is depicted in Scheme 1. All three photoacids were synthesized starting from 1,8-naphthalic anhydride by sulfonation with fuming sulfuric acid to give sodium-1,8-naphthalic anhydride-3,6-disulfonate.[37] The disulfonate was converted to either potassium-3-hydroxy-1,8-naphthalic anhydride-6-sulfonate or 3,6-dihydroxy-1,8-naphthalic anhydride by reaction with molten KOH at 200−250 °C. The main product was either the mono- or dihydroxy compound depending on the reaction time. Reaction with a primary amine (diethylene glycolamine or glycine methyl ester) yielded the corresponding 1,8-naphthalimides. Hydrolysis of the ester under basic conditions afforded the corresponding carboxylic acid. Detailed descriptions of the synthetic procedures and characterizations of the compounds are given in the Supporting Information. Other used materials are also described in the Supporting Information.

Spectroscopic Measurements. All NMR spectra were recorded using a Bruker Avance 400 or DRX 500 spectrometer. IR spectra were recorded using a Bruker Alpha-P spectrometer.

Steady-state absorption and fluorescence spectra were recorded using a Shimadzu UV-2700 spectrophotometer and a SPEX Fluorolog3-22 fluorimeter, respectively. The fluorescence spectra were collected in a right-angle geometry and corrected for the spectral sensitivity of the instrument. All measurements were carried out at room temperature (21 ± 1 °C). The concentrations of the samples were 7−120 μM. Quantum yields were determined using quinine sulfate (>99%, Fluka) in 0.5 M H_2SO_4 (aq.) as a quantum yield standard with $\Phi_f = 0.55$.[38,39]

Experimental setups for time-resolved (TCSPC and flash photolysis) and other (pH and Karl Fischer) measurements are described in the Supporting Information.

Theoretical Calculations. All calculations were performed with the ADF2013 software[40,41] using the PBE0 functional[42,43] and the TZ2P[44] basis set. We chose the PBE0 functional because it has been shown to produce reasonable results for 1,8-naphthalimide dyes.[45,46] The conductor-like screening model (COSMO)[47] was used to include solvent effects for all DFT and TD-DFT calculations.

RESULTS

Steady-State Measurements in Aqueous Solutions. Ground-state pK_a values were determined by measuring absorption spectra over a broad pH range. Mild buffer solutions (c = 5−10 mM) were used for intermediate pH values (pH 3.0−10.5). Aqueous H_2SO_4 or NaOH were used for lower and higher pH ranges, respectively. The absorption spectra of **EG-dHONI** show a clear conversion from the neutral to the anionic form with an isosbestic point at λ = 402 nm. A second isosbestic point was observed at λ = 317 nm, but the last four spectra measured at the highest pH values deviated slightly from this point. The reason for the deviation is most likely minor hydrolysis (ring opening of the imide group) at high pH which will be discussed later. Interestingly, the absorption spectrum of **EG-SHONI** showed splitting of the main absorption band into two bands (see Figure 9). Both bands

dx.doi.org/10.1021/jp508334s | J. Phys. Chem. B 2015, 119, 2515−2524

were red-shifted upon conversion to the anionic form (Supporting Information).

Concentrations of the neutral and anionic forms were calculated using the Lambert−Beer law at two selected wavelengths close to the absorption maxima of the neutral ($\lambda_{ROH} \approx 380$ nm) and anionic forms ($\lambda_{RO^-} \approx 440$ nm). Ground-state pK_a values were estimated from the midpoints of the molar fraction data. Absorption spectra of **EG-dHONI** at different pH values are presented in Figure 1. Absorption spectra of **COOH-dHONI** and **EG-SHONI** are shown in Figures S1 and S2, respectively (Supporting Information).

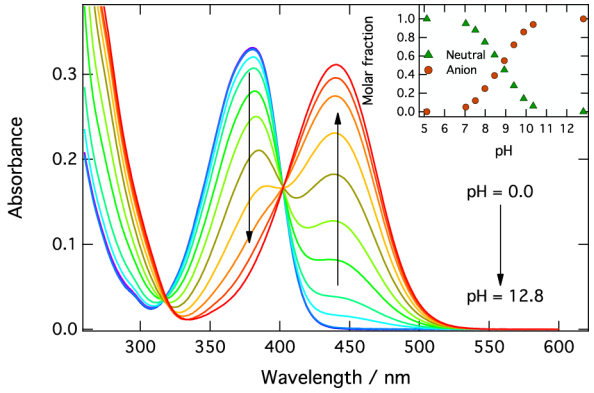

Figure 1. Absorption spectra of **EG-dHONI** (c = 30 μM) at different pH values. The inset shows the molar fractions of the neutral and anionic forms as a function of pH.

Excited-state pK_a values were estimated using the Förster cycle.[48,49] Absorption and emission spectra of the neutral form were measured in 2 M H_2SO_4, and aqueous NaOH (pH ≈ 11−12) was used for the spectra of the anionic form. Emission of the anion was measured upon direct excitation of the anion absorption band at ∼440 nm. The emission spectra measured in 2 M H_2SO_4 still exhibited anion emission, but this should not significantly affect the emission maxima of the neutral band. The anion emission in this solvent was strongest for **EG-SHONI** and weakest for **EG-dHONI**. We used an average of absorption and emission maxima as the 0−0 transitions, $\bar{\nu}_{00} = (\bar{\nu}_{abs}^{max} + \bar{\nu}_{em}^{max})/2$. Absorption and emission spectra of the neutral and anionic forms of **EG-dHONI** are presented in Figure 2. Spectra of **COOH-dHONI** and **EG-SHONI** are given in Figures S3 and S4, respectively (Supporting Information).

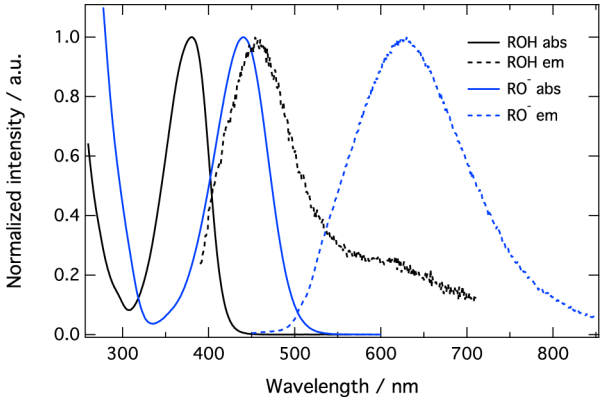

Figure 2. Normalized absorption and emission spectra of the neutral and anionic forms of **EG-dHONI** in aqueous solutions.

Absorption maxima and molar absorption coefficients of the neutral and anionic forms and ground- and excited-state pK_a values are summarized in Table 1.

Fluorescence Spectra and Quantum Yields in H_2O and Organic Solvents. Excited-state deprotonation in water and protic and aprotic organic solvents was studied by means of steady-state fluorescence spectroscopy. Emission spectra and quantum yields (Φ_f) were measured in H_2O, MeOH, EtOH, 2-PrOH, *n*-BuOH, and DMSO. The emission spectra were fitted with a sum of skewed gaussians (eq 1) to decompose the quantum yields for neutral and anionic forms.[50,51] Two skewed gaussians were sufficient to adequately model the emission spectra in water and alcohols, whereas a sum of three skewed gaussians was required for samples in DMSO.

$$I(\lambda) = Y\begin{cases}\exp[-\ln(2)\{\ln(1+\alpha)/b\}^2] & \alpha > -1\\ 0 & \alpha \le -1\end{cases} \quad (1)$$

$$\alpha = \frac{2b(x - x_0)}{\Delta x} \quad (2)$$

In eqs 1 and 2, Y is the peak intensity, x_0 the peak position, Δx the bandwidth, and b the asymmetry parameter. Normalized emission spectra of **EG-dHONI** in organic solvents are presented in Figure 3. The spectra of **COOH-dHONI** and **EG-SHONI** are given in Figures S5 and S6, respectively (Supporting Information). The spectrum in water (Figure S7, Supporting Information) is left out to allow better comparison between the spectra in organic solvents. Representative fits of the emission spectra of **EG-dHONI** in DMSO with a sum of two or three skewed gaussians are given in Figures S8 and S9, respectively (Supporting Information).

Following the analogy presented by Jung et al.,[16] the ratio Φ_{ROH}/Φ_{RO^-} follows the same trend as the pK_a^* and reflects the efficiency of deprotonation. The assumption should be valid for a set of similar compounds with similar fluorescence lifetimes and quantum yields in a certain solvent. The ratios for all three compounds in different solvents are presented in Figure 4. The total quantum yields, fraction of total emission attributed to ROH*, and ratios of the neutral and anion fluorescence quantum yields are summarized in Table 2.

Fluorescence quantum yields in water were dependent on pH but were Φ_f < 0.5% in all cases. Quantum yields increased from 2 M H_2SO_4 to pH 3 but remained constant at pH 3−7. Also, the ratio Φ_{ROH}/Φ_{RO^-} was dependent on the pH but did not change significantly at pH 3−7 upon excitation of the neutral form. Normalized emission spectra of **EG-dHONI** at different pH values are shown in Figure S7 (Supporting Information).

Time-Resolved Fluorescence in DMSO. Deprotonation kinetics of all compounds were studied in DMSO with the TCSPC method. Samples were found to be unstable in the presence of oxygen upon laser irradiation and were thus deoxygenated by argon bubbling. The decay of the neutral form was monitored with λ_{mon} = 430 nm with a 10 ns time window and fitted with a three-exponential model (eq S1 with n = 3, Supporting Information). The decay of the anion was monitored with λ_{mon} = 610 nm with a 50 ns time window and fitted with a two-exponential model (eq S1 with n = 2, Supporting Information). Decays of **EG-dHONI** together with the instrument response function are presented in Figure 5, and decays of **COOH-dHONI** and **EG-SHONI** are shown in

dx.doi.org/10.1021/jp508334s | J. Phys. Chem. B 2015, 119, 2515−2524

Table 1. Absorption Maxima and Molar Absorption Coefficients of the Neutral and Anionic Forms and Ground- and Excited-State pK_a Values

compound	λ^{max}_{ROH} (nm)	ε^{max}_{ROH} (M^{-1} cm^{-1})	$\lambda^{max}_{RO^-}$ (nm)	$\varepsilon^{max}_{RO^-}$ (M^{-1} cm^{-1})	pK_a	pK_a^*	ΔpK_a
EG-dHONI	381	11000 ± 300	440	10400 ± 400	8.8 ± 0.1	−1.2	−10.0
COOH-dHONI	382	11300 ± 400	439	10300 ± 400	8.8 ± 0.1	−1.4	−10.3
EG-SHONI	384	6100 ± 200	444	5000 ± 200	8.0 ± 0.1	−1.9	−9.9

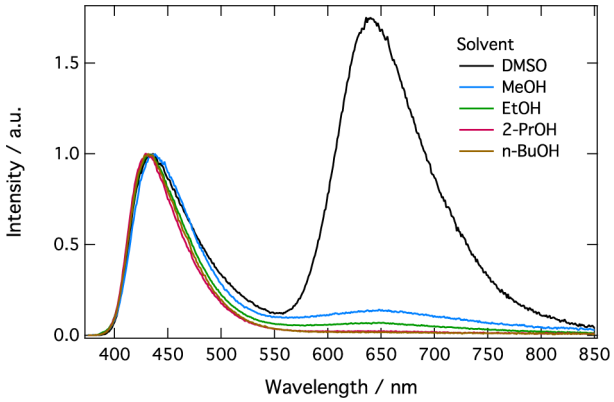

Figure 3. Normalized emission spectra of **EG-dHONI** in organic solvents (λ_{ex} = 360 nm).

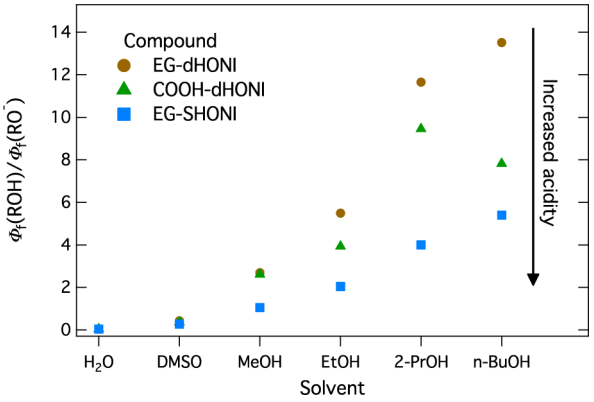

Figure 4. Ratios of neutral and anion fluorescence quantum yields of all three compounds in organic solvents.

Figures S10 and S11, respectively (Supporting Information). All the fitting results are summarized in Table 3.

All compounds exhibited a fast component (τ_1 < 25 ps = IRF) at the neutral band. The component with the largest amplitude had a lifetime of τ_2 = 620−860 ps. The rise of the anion emission at 610 nm showed a similar lifetime but seemed somewhat faster. Also, the amplitude associated with the rise time was only ∼50% of the total amplitude of the positive

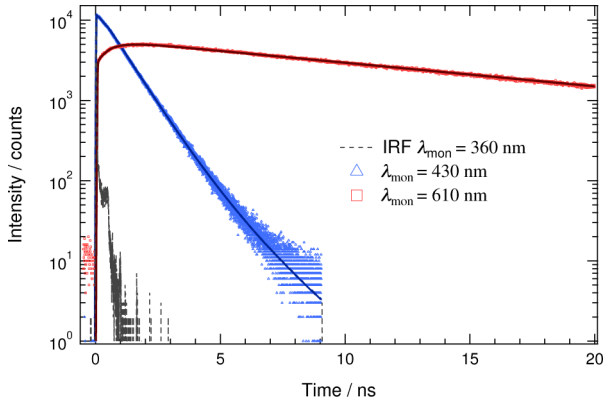

Figure 5. Decays of the neutral (λ_{mon} = 430 nm) and anionic (λ_{mon} = 610 nm) forms of **EG-dHONI** in DMSO. The excitation wavelength was 360 nm.

component. In addition, the neutral region exhibited a longer-lived tail with a small amplitude (α_3 < 4%). The anion emission showed long-lived decay with a lifetime of τ_2 = 14.6−16.7 ns. All decay traces were well described by the multiexponential model and χ^2 < 1.13 in all cases.

Time-Resolved Fluorescence of EG-dHONI in Aqueous Solutions at Different pH Values. Excitation of **EG-dHONI** in acidic aqueous solutions led to emission of the neutral and anionic forms, which were monitored at λ_{mon} = 420−480 nm and λ_{mon} ≈ 530−630 nm, respectively. In this case, the samples were photostable and deoxygenation was unnecessary. The decay traces were fitted with three- (in 0.5 M H_2SO_4) or four-exponential (pH 3.0, 4.8, and 6.5) models with global lifetimes (eq S1 with n = 3 or 4, Supporting Information). Representative decay associated spectra (DAS) at pH 4.8 are presented in Figure 6. The DAS in 0.5 M H_2SO_4 and at pH 3.0 and 6.5 are shown in Figures S12−S14 (Supporting Information). Individual decay traces at selected wavelengths for all samples are shown in Figures S15−S18 (Supporting Information). The fitting results are summarized in Table 4.

All DAS exhibited a fast component with τ_1 < 25 ps as the main decay component in the neutral region. The same component also appeared as a rise time in the anion spectral range. In addition, all spectra showed an intermediate

Table 2. Total Quantum Yields (Φ_f), Fraction of Total Emission Attributed to ROH* (α_{ROH}), and Ratios of the Neutral and Anion Fluorescence Quantum Yields of the Studied Compounds in a Series of Solvents

	EG-dHONI			COOH-dHONI			EG-SHONI		
solvent	Φ_f	α_{ROH}	Φ_{ROH}/Φ_{RO^-}	Φ_f	α_{ROH}	Φ_{ROH}/Φ_{RO^-}	Φ_f	α_{ROH}	Φ_{ROH}/Φ_{RO^-}
H_2O	<0.005	4.8%	0.05	<0.005	4.6%	0.05	<0.005	3.6%	0.04
DMSO	0.17	30%	0.43	0.17	26%	0.36	0.17	22%	0.28
MeOH	0.01	73%	2.70	0.02	72%	2.61	0.01	51%	1.05
EtOH	0.03	85%	5.49	0.03	80%	3.93	0.03	67%	2.04
2-PrOH	0.06	92%	11.7	0.05	90%	9.45	0.06	80%	4.00
n-BuOH	0.06	93%	13.5	0.05	89%	7.82	0.06	84%	5.40

dx.doi.org/10.1021/jp508334s | J. Phys. Chem. B 2015, 119, 2515−2524

Table 3. Decay Times τ and Amplitudes α of the Decays of All Photoacids in DMSO

	neutral (λ_{mon} = 430 nm)				anion (λ_{mon} = 610 nm)		
compound	τ_1 (α_1) (ps)	τ_2 (α_2) (ps)	τ_3 (α_3) (ns)	χ^2	τ_1 (α_1) (ps)	τ_2 (α_2) (ns)	χ^2
EG-dHONI	<25 (22%)	860 ± 40 (74%)	1.6 ± 0.1 (4%)	1.04	650 ± 80 (−43%)	14.7 ± 0.1 (100%)	1.09
COOH-dHONI	<25 (37%)	740 ± 30 (60%)	1.8 ± 0.2 (3%)	1.08	540 ± 80 (−47%)	14.6 ± 0.1 (100%)	1.03
EG-SHONI	<25 (17%)	620 ± 20 (82%)	3.4 ± 0.4 (1%)	1.13	450 ± 60 (−62%)	16.7 ± 0.2 (100%)	1.02

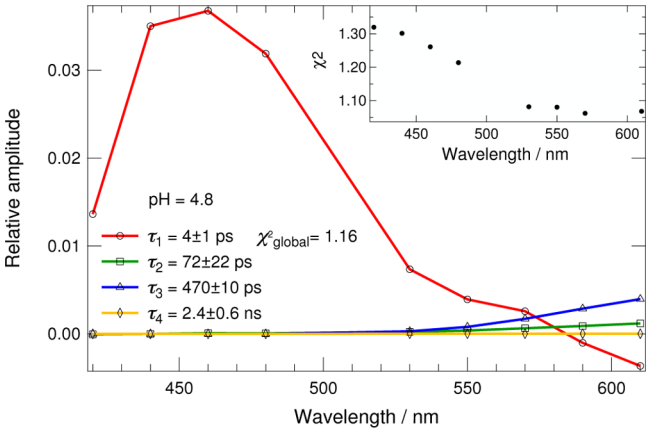

Figure 6. Decay associated spectra of **EG-dHONI** at pH 4.8. The excitation wavelength was 380 nm. The inset shows the individual χ^2 values.

Table 4. Global Lifetimes and χ^2 Values of the Fittings of EG-dHONI in Aqueous Solutions at Different pH Values

solvent	τ_1 (ps)	τ_2 (ps)	τ_3 (ps)	τ_4 (ns)	χ_{glob}^2
0.5 M H_2SO_4	<25	73 ± 2		1.7 ± 0.3	1.15
pH 3.0	<25	74 ± 17	470 ± 10	3.6 ± 0.4	1.14
pH 4.8	<25	72 ± 22	470 ± 10	2.4 ± 0.6	1.16
pH 6.5	<25	80 ± 24	470 ± 10	2.0 ± 0.4	1.13

component with $\tau_2 \approx 75$ ps. In 0.5 M H_2SO_4, this component had positive amplitude in both the neutral and anion bands, whereas at pH 3.0−6.5 the component had positive amplitude only in the emission range of the anion. The DAS at pH 3.0−6.5 were almost identical, as expected based on the equal quantum yields in this pH range, and exhibited a third intermediate component with τ_3 = 470 ps. All spectra showed a longer-lived tail with very small amplitude (<1%) throughout the whole wavelength range. The decay traces were very well described by the multiexponential model in the anion wavelength range in all cases. The χ^2 values were less satisfactory (~1.2−1.3) in the neutral region. This was due to the fast component (faster than IRF) and the long-lived tail, which was not that well described by the exponential function and will be discussed later.

Decays of the Ground-State Anion of EG-dHONI at Different pH Values. The decay of the ground-state anion formed after excited-state deprotonation at different pH values (pH 3.0, 5.0, and 7.0) was studied by nanosecond transient absorption (flash photolysis). Samples were deoxygenated by argon bubbling to avoid photodegradation under intense laser excitation (E = 1.5−2.5 mJ/pulse). The transient spectra showed induced absorption with λ_{max} = 440 nm corresponding to the anion band. The spectra also showed the emission of the anion in the first trace at t = 0 ns. The transient spectra are shown in Figures S19−S21 (Supporting Information). Decay traces were obtained by averaging the signal at λ = 438−442 nm and are presented in Figure 7. The concentration of the anion was calculated on the basis of the molar absorption coefficient (see Table 1).

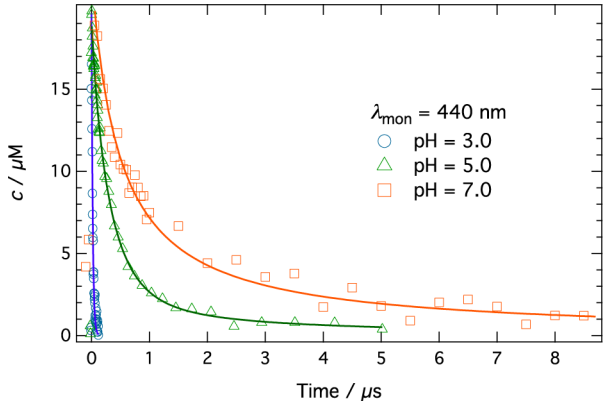

Figure 7. Decays of the ground-state anion monitored at 440 nm at different pH values. The excitation wavelength was 380 nm.

The decay at pH 3.0 was fitted with a single-exponential function (pseudo-first-order reaction). At intermediate pH 5.0 ($[H^+]_0 \approx [H^+]_{jump}$), the decay was modeled with a function derived by Huppert et al. for recombination at intermediate pH values (eq 17 in ref 36). The model consists of a mixture of first- and second-order terms, and the initial proton concentration, $[H^+]_0$, is used as a fitting parameter. The decay at pH 7.0 is modeled as pure second-order bimolecular recombination. The fitting results are summarized in Table 5. The decays are very well described by the chosen models.

Table 5. Fitting Results of the Decays of the Ground-State Anion of EG-dHONI at Different pH Values

pH	τ^a (ns)	$k_{bimol}{}^b$ ($\times 10^{11}$ M^{-1} s^{-1})
3.0	23 ± 2	
5.0		1.8 ± 0.1
7.0		1.9 ± 0.1

[a]From single-exponential function. [b]Bimolecular recombination rate.

Possibility of the Formation of the Dianion of EG-dHONI. The possibility of deprotonating both hydroxyl groups of **EG-dHONI** under basic conditions was studied with UV−vis and NMR spectroscopy. The absorption spectrum showed time-dependent conversion of the anion absorption to a short-wavelength absorbing species (λ_{max} = 354 nm) in 1 M NaOH with isosbestic points at λ = 311 and 376 nm. The fully converted sample still showed a residual absorption band at ~440 nm. The rate of the conversion was obtained by fitting the absorption of the anion (at 440 nm) vs time with a seventh order polynomial function and taking the first derivative of the fit. The so-called graphical rate equation is obtained by plotting the derivative (i.e., rate) as a function of the absorption (i.e.,

dx.doi.org/10.1021/jp508334s | J. Phys. Chem. B 2015, 119, 2515−2524

concentration), and it exhibits pseudo-first-order kinetics demonstrated by the linear relationship.[52] The absorption spectra of the conversion are presented in Figure 8, and the graphical rate equation is shown in the inset together with a linear fit.

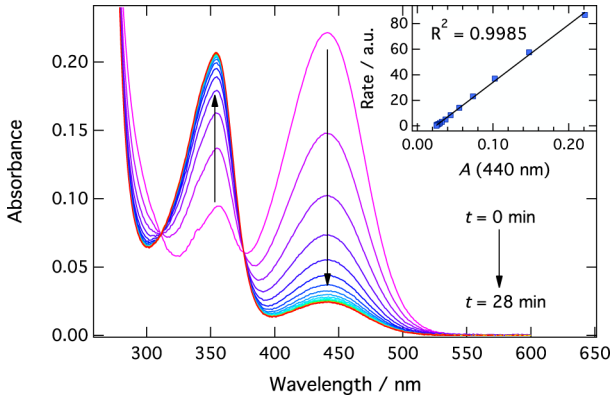

Figure 8. Absorption spectra of **EG-dHONI** in 1 M NaOH as a function of time. The inset shows the graphical rate equation of the conversion.

The reversibility of the observed changes was studied by acidification of the sample after complete conversion. Gradual acidification revealed multiple absorbing species at intermediate pH values (pH 4−10) eventually (at pH < 2) resulting in an absorption spectrum of the neutral form with 3 nm blue shift (compared to the original absorption) and slightly increased absorption in the UV region (results not shown). The final product after acidification was concluded to be 3,6-dihydroxy-1,8-naphthalic anhydride confirmed by reference UV−vis measurements. Moreover, ^{1}H NMR experiments showed that the naphthalimide undergoes a ring opening reaction under strongly basic conditions, forming a deprotonated carboxylic acid and amide groups. The amide group was cleaved upon acidification, and eventually, a ring closing reaction took place to form the anhydride under strongly acidic conditions (results not shown). Different forms of the naphthalimide and naphthalic anhydride as a function of pH together with the absorption maxima are shown in Scheme S1 (Supporting Information).

Quantum Chemical Calculations on Model Compounds. We used quantum chemical calculations to study the nature of the excited state resulting in photoacidity and to compare the effect of substitution. This was done by looking at the frontier orbitals and by comparing the Mulliken charges on the hydroxyl oxygen between optimized ground and excited states, respectively. In addition, we used TD-DFT to calculate the absorption and emission spectra of the model compounds. Calculations consisted of geometry optimizations and vertical transitions in both the ground and excited states. We chose four model compounds, namely, *N*-methyl-3,6-dihydroxy- (**dHONI**), *N*-methyl-3-hydroxy-6-sulfonate- (**SHONI**), *N*-methyl-3-hydroxy-6-cyano- (**6CNHONI**), and *N*-methyl-3-hydroxy-5-cyano-1,8-naphthalimides (**5CNHONI**); see Scheme 1 for numbering. The cyano compounds were included to compare the influence of different substituents (−OH, $-SO_3^-$, and −CN) and the position (5 vs 6) of the substituent.

All calculations showed that the two lowest-energy absorption bands originate from $\pi \rightarrow \pi^*$ transitions from HOMO−1 and HOMO to LUMO. In sulfonate- and cyano-functionalized compounds, the splitting of the two bands was greater compared to **dHONI** (~0.6 eV vs ~0.1 eV). In the experimental spectra, the two bands of **EG-SHONI** are clearly separated, whereas **EG-dHONI** exhibits only a single main band with a small shoulder/broadening at shorter wavelength. The calculated and experimental absorption spectra of **dHONI** and **SHONI** are presented in Figure 9.

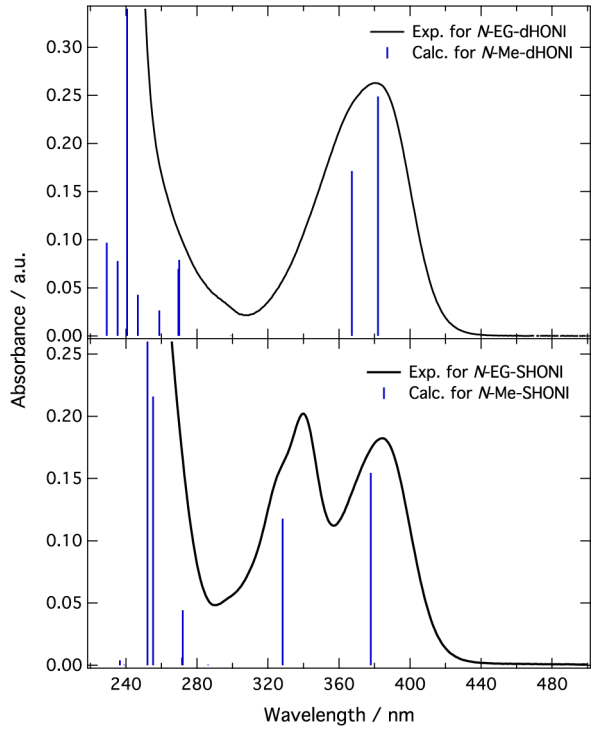

Figure 9. Calculated (for *N*-methyl-) and experimental (for *N*-EG-) absorption spectra of the neutral forms of **dHONI** and **SHONI**.

The frontier orbitals of **dHONI** are presented in Figure 10, and those of **SHONI**, **5CNHONI**, and **6CNHONI** are shown in Figures S22−S24, respectively (Supporting Information). The frontier orbitals showed diminished electron density on the hydroxyl oxygen in the first excited state (HOMO → LUMO) in all cases. This was also quantified by comparing the Mulliken charges of the hydroxyl oxygen between the optimized ground and excited states. All compounds showed decreased negative charge on the hydroxyl oxygen in the excited state. The magnitude of the change was relatively small and showed the trend **SHONI** < **dHONI** < **5CNHONI** < **6CNHONI**. Similar trends were also observed in corresponding C−O and O−H distances, but the differences were small (results not shown). All the parameters are summarized in Table 6.

DISCUSSION

Steady-State Measurements in Aqueous Solutions. **EG-dHONI** and **COOH-dHONI** exhibit their main absorption bands at ~380 nm with equal molar absorption coefficients. **EG-SHONI** exhibits two main bands, lower and higher in energy, with molar absorption coefficients roughly half of those observed for the dihydroxy compounds. The main absorption bands were shown to originate from HOMO−1 and HOMO to LUMO transitions. In **EG-dHONI** and **COOH-dHONI**, the two bands are merged to a single broad absorption, resulting in

dx.doi.org/10.1021/jp508334s | J. Phys. Chem. B 2015, 119, 2515−2524

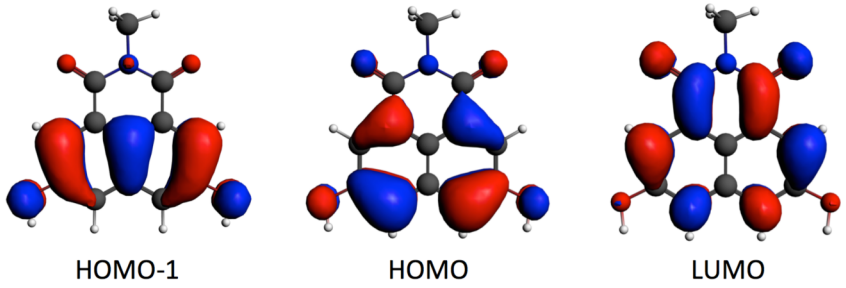

Figure 10. Frontier orbitals of **dHONI** calculated on the ground-state geometry with the PBE0/TZ2P level of theory.

Table 6. Calculated and Experimental Absorption and Emission Energies (in eV) and Changes in the Mulliken Charges on the Hydroxyl Oxygen upon Excitation

compound	E_{abs}^{calc}	E_{abs}^{exp}	E_{em}^{calc}	E_{em}^{exp}	E_{0-0}^{calc}	E_{0-0}^{exp}	$\Delta q(O)_{ES-GS}$
SHONI	3.28	3.23	3.02	2.66	3.15[b]	2.94[b]	0.007[c]
dHONI	3.25	3.26	2.94	2.68	3.09[b]	2.97[b]	0.008[c]
5CNHONI	3.08	*a*	2.71	*a*	2.89[b]	*a*	0.010[c]
6CNHONI	3.22	*a*	2.88	*a*	3.05[b]	*a*	0.022[c]

[a]Experimental data not available. [b]Average of absorption and emission maxima. [c]Change in Mulliken charge of the hydroxyl oxygen.

roughly a 2 times higher absorption coefficient compared to **EG-SHONI**. The anion bands show ~60 nm red shifts compared to those of the neutral compounds in all molecules. Emission spectra of all compounds show nearly mirror-image emission bands in the wavenumber domain, but the anionic form exhibits a substantially larger Stokes shift (~4600 cm^{-1} vs ~7000 cm^{-1} for **EG-dHONI**).

The ground-state pK_a is not affected by *N*-substitution, whereas the aromatic sulfonate substituent decreases the pK_a by 0.8 units. The excited-state pK_a is affected both by *N*- and aromatic substitution, but the changes are relatively small (0.7 pK_a units). The main reason for the lower pK_a^* of **EG-SHONI** is the decreased ground-state pK_a. Actually, **EG-SHONI** exhibits the smallest ΔpK_a upon excitation. The pK_a^*'s follow the trend **EG-SHONI** < **COOH-dHONI** < **EG-dHONI**, also supported by the ratios of the neutral and anion emission intensities in 2 M H_2SO_4.

Fluorescence Spectra and Quantum Yields in H_2O and Organic Solvents. The fluorescence quantum yields (Table 2) of all compounds are very low in H_2O (<0.5%) and alcohols (≤6%). This can be attributed to proton quenching.[53] After ESPT, the proton recombination results in efficient deactivation of the excited state which is enhanced in more proton rich solvents such as water or methanol. Another quenching mechanism, reported for 1-naphthol,[53,54] is protonation of the aromatic ring system in the excited state. Indeed, we observed deuteration of the H_4 and H_5 for **EG-dHONI** and **COOH-dHONI** and H_4 for **EG-SHONI** under basic conditions upon heating in D_2O in our NMR-experiments, but we could not reproduce this exchange photochemically (results not shown) under similar conditions (pH 3, UV-irradiation) as reported for 1-naphthol. Therefore, the protonation of the ring system does not play a role in the excited-state processes of the present compounds. Protonation of the carbonyl group[55] could also be a possible quenching mechanism, but it would be difficult to separate experimentally from the other proton quenching mechanisms. In aprotic solvents, such as DMSO, the fluorescence quantum yield is significantly higher (17%).

The ratios of the neutral and anion fluorescence quantum yields of the studied compounds correlate with the pK_a^*'s in all studied solvents. Although the ratio in a certain solvent allows comparison between similar compounds, it does not necessarily reflect the absolute value of pK_a^* due to differences in quantum yields and lifetimes of the neutral and anionic forms in different solvents. Similarly, the percentage of the neutral emission reflects the amount of deprotonation and thus the pK_a^*. Interestingly, the sum of two skewed gaussians was adequate to describe the emission spectra in aprotic solvents, whereas three were required for samples in DMSO. This is attributed to the much higher concentration of the intermediate proton-transfer species, the contact ion pair, as will be discussed below.

Time-Resolved Fluorescence in DMSO. The decays in DMSO (Table 3) can be explained by a two-step deprotonation process (Scheme 2). This gives rise to a two-exponential decay in the neutral region. The fastest component (τ_1 < 25 ps) in all cases corresponds to the initial relaxation to the equilibrium between the neutral form and the contact ion pair. The lifetime reflects the sum of the forward (k_{diss}) and backward (k_{rec}) rates of the initial step but is too fast (<IRF) for quantitative analysis of the rate constants. The second component (τ_2 = 620−860 ps) is the decay of the equilibrium state resulting in formation of the free ion pairs. This component has the largest amplitude in the neutral region, indicating that the equilibrium state has a significant population of the neutral form. The decay of the equilibrium state correlates with pK_a^*, i.e., is fastest for the strongest excited-state acid (**EG-SHONI**). This is most likely the result of a lower energy barrier for the diffusion controlled proton dissociation. Attachment of electron withdrawing groups on the aromatic system will increase the extent of intramolecular charge transfer (and acidity), leaving the oxygen less negatively charged.[54] Thus, the Coulombic barrier for the escape of the proton is lowered, resulting in faster decay of the intermediate contact ion pair. The long-lived tail (τ_3 = 1.6−3.4 ns) with minor amplitude originates most likely from the geminate proton recombination,[56,57] although this largely results in fluorescence quenching at least in protic solvents. Another possibility is minor impurities due to photo-degradation processes.

The rise times of the anion emissions show a similar trend as the decays of the equilibrium state but are ~200 ps shorter than the decays observed in the neutral region. Moreover, the

dx.doi.org/10.1021/jp508334s | J. Phys. Chem. B 2015, 119, 2515−2524

negative amplitudes are only half of the positive counterparts. This can be partly attributed to the large overlap between the emission of the contact ion pair and the free ion pair at the monitoring wavelength (610 nm). In the spectral-line-shape analysis of **EG-dHONI**, the intermediate emission band centered at ~636 nm can be attributed to the contact ion pair (Figure S9, Supporting Information) and has ~20% intensity of the major emission band attributed to the free ion pair. This would result in observation of roughly −80% negative amplitude in the time-resolved experiments at this monitoring wavelength. This means that part of the anions are formed directly during the IRF and only part via the intermediate state, namely, the contact ion pair. The disagreement between the lifetimes of the intermediate component could arise from the poorly resolved initial decay mixed with the intermediate component especially in the anion spectral range. The long-lived component (τ_3 = 14.6−16.7 ns) in the anion emission band corresponds to the decay of the anion.

A more sophisticated three-step deprotonation model has been proposed by Huppert et al.[33,57] and also discussed by us in a previous publication[58] which could explain the disagreement between the lifetimes and amplitudes of the rise and decay components. In this model, an additional species, namely, the solvent separated ion pair, is introduced, which results in an additional decay component. Thus, the anion spectral range should be fitted with a four-exponential model (initial relaxation to equilibrium, contact ion pair, solvent separated ion pair, and free ion pair). Our data, however, were adequately fitted already with the two-exponential model. In addition, the best spectral fittings were achieved already with three spectral-line-shape functions supporting the two-step deprotonation model. More thorough measurements over a wider wavelength range would be required for full spectral and kinetic separation of all the overlapping components and is out of the scope of the present study.

Time-Resolved Fluorescence of EG-dHONI in Aqueous Solutions at Different pH Values. The decays of **EG-dHONI** in aqueous solutions (Table 4) can also be modeled by the two-step deprotonation mechanism. Similarly to results in DMSO, the ultrafast component (τ_1 < 25 ps) corresponds to the initial relaxation of the neutral form to equilibrium between the contact ion pair followed by decay of the equilibrium state ($\tau_2 \approx$ 75 ps). In 0.5 M H_2SO_4, the equilibrium state has a minor population of the neutral form, whereas at pH 3−7 the equilibrium is completely on the side of the contact ion pair and the first step in Scheme 2 can be considered unidirectional, i.e., $k_{diss} = 1/\tau_1$. Moreover, in 0.5 M H_2SO_4, no free ion pairs are formed due to the high proton concentration of the bulk solvent. At higher pH, the anion decays with τ_3 = 470 ps, independent of the pH. In addition, all samples exhibit a longer-lived component with very small amplitude attributed to the geminate recombination[56,57] or minor populations of photodegradation products. The fittings are very good in the anion emission range but much worse in the neutral range. This can be attributed to the limited time resolution of our instrument and inadequate fittings of the long-lived tails.

The model presented in Scheme 2 is qualitatively in good agreement with the data, but the limited time resolution of our TCSPC setup hinders the quantitative analysis of the rate constants. Faster techniques (fs-pump−probe or up-conversion) have been used to resolve these ultrafast components in related studies on photoacids.[15,33,57,59,59,60] Another approach is to use mixtures of organic solvents and water to slow down the deprotonation kinetics.[58]

Decays of the Ground-State Anion of EG-dHONI at Different pH Values. The diffusion controlled back-protonation of the ground-state anion (Table 5) is well described in the literature.[35,36] At low pH, the back-protonation exhibits pseudo-first-order kinetics also reported for **HPTS** at low pH. Fitting to an exponential function gives a lifetime of τ = 23 ns at pH 3.0. The decay at intermediate pH is fitted as a mixture of first- and second-order reactions with an equation derived by Huppert et al.[36] The pH of the sample was measured prior to deoxygenation, but the initial proton concentration was used also as a fitting parameter. The pH was 5.0 after sample preparation, but the proton concentration resulting from the fittings gave pH 5.4, indicating a slight increase in pH during deoxygenation. The second-order rate constant at pH 5.4 is $k_{bimol} = 1.8 \times 10^{11}$ M^{-1} s^{-1}. The decay at neutral pH exhibits pure diffusion limited bimolecular recombination with $k_{bimol} = 1.9 \times 10^{11}$ M^{-1} s^{-1}. The rate at neutral pH is comparable to that of **HPTS** (K^0_{bimol} = (1.84−2.06) × 10^{11} M^{-1} s^{-1})[35] at zero ionic strength.

Possibility of the Formation of the Dianion of EG-dHONI. No dianion was observed in any of the experiments. The compound undergoes hydrolysis of the imide group under strongly basic conditions before deprotonation of the second hydroxyl group is observed. Deprotonation of the first hydroxyl group increases the pK_a of the second hydroxyl group deactivating the deprotonation both in the ground and excited states in the studied pH range. Similar observations have been reported for 4,5-dihydroxynaphthalene-2,7-disulfonic acid (chromotropic acid).[61] For chromotropic acid, the pK_a of the second hydroxyl group was found to be 15.6 without any photoacid character.

Quantum Chemical Calculations on Model Compounds. Quantum chemical calculations (Table 6) reproduce the absorption spectra of **EG-dHONI** and **EG-SHONI** to high accuracy (ΔE < 0.06 eV), supporting the choice of functional and basis set. Calculated emission energies are overestimated by ~0.2−0.4 eV. This could be due to the explicit solvent effects such as hydrogen bonding and solvation of the hydrogen bonded complex in the excited state.[18] Although the bond lengths (C−O and O−H) are slightly altered in the excited state, the changes are negligibly small in the absence of a hydrogen bond or proton acceptor. An explicit solvent model combined with COSMO could possibly overcome these limitations but was out of the scope of the present study.

Frontier orbitals show the partial charge transfer character of the excited state resulting in photoacidity. The electron density of the hydroxyl oxygen is significantly decreased in the first excited state (HOMO → LUMO). The change in the Mulliken charge of the hydroxyl oxygen upon excitation possibly correlates with ΔpK_a (**SHONI** < **dHONI**), but more experimental data is required to establish stronger correlation. Nevertheless, the calculations suggest that attachment of a cyano group in the 6-position should strongly enhance the photoacidity. Similar experimental observations have been reported for cyano-functionalized 2-naphthols.[12,21]

CONCLUSIONS

We have studied both ground- and excited-state acid−base properties of three novel **NI**-derived "super" photoacids exhibiting negative pK_a^*'s. The pK_a is not altered by *N*-substitution but is decreased upon sulfonation of the aromatic

dx.doi.org/10.1021/jp508334s | J. Phys. Chem. B 2015, 119, 2515−2524

system. The ΔpK_a's of all three compounds are comparable, and a decrease in pK_a^* is mainly achieved by decreasing the ground-state pK_a. Quantum chemical calculations and experimental data on related compounds suggest[12,21] that attachment of cyano groups could further enhance the photoacidity.

All studied compounds are deprotonated upon excitation in alcohols and DMSO. Good correlation is established between the pK_a^* and the ratio of the neutral and anion fluorescence quantum yields in a certain solvent. Quantum yields are small in protic solvents, which is attributed to the proton quenching process, whereas the fluorescence is restored in aprotic solvents such as DMSO.

The deprotonation process both in DMSO and H_2O can be reasonably well explained with the two-step deprotonation model (Scheme 2). The first step corresponds to the initial relaxation to the equilibrium state between the neutral form and contact ion pair followed by a diffusional step resulting in the formation of the free ion pairs (at pH $\geq$ 3). The rate of decay of the equilibrium state in DMSO also correlates with pK_a^* in this series of compounds. Slight disagreement in the data measured in the neutral vs anion wavelength ranges suggests a more complicated deprotonation mechanism (three-step model), but the initial processes are too fast (<25 ps) to be resolved in our experiments.

Our results support and complement the already available body of knowledge and understanding of photoacids reported in the literature. Nevertheless, these photoacids extend the ongoing field of research on "super" photoacids and offer robust and easily modifiable compounds with tunable acid–base (both ground and excited states), spectroscopic, and chemical properties. The substituent on the imide group offers a convenient site for linking the photoacid to any substrate of interest (inorganic, organic, or biological), or it can be used to tune the solubility from water all the way to nonpolar solvents. Moreover, the present compounds are suitable for pH-jump experiments where ground-state $pK_a > 7$ is desirable. The dihydroxy compounds are almost fully in their neutral form in the ground state under physiological pH (pH $\approx$ 7.4) and could be suitable for biological applications. More detailed studies on a larger set of compounds and with better time resolution are required to establish better correlations between the parameters influencing the photoacidity and to fully resolve the initial steps in the deprotonation mechanism.

■ ASSOCIATED CONTENT

Supporting Information

Synthetic procedures and characterization of the compounds, experimental information, additional spectra of the photoacids, scheme of different species of **EG-dHONI** as a function of pH, and additional frontier orbitals. This material is available free of charge via the Internet at http://pubs.acs.org.

■ AUTHOR INFORMATION

Corresponding Author

*E-mail: a.m.brouwer@uva.nl.

Notes

The authors declare no competing financial interest.

■ ACKNOWLEDGMENTS

This research was financially supported by The Netherlands Organisation for Scientific Research (NWO).

■ REFERENCES

(1) Förster, T. Fluoreszenzspektrum und Wasserstoffionenkonzentration. *Naturwissenschaften* **1949**, *36*, 186–187.
(2) van Oort, B.; ter Veer, M. J. T.; Groot, M. L.; van Stokkum, I. H. M. Excited State Proton Transfer in Strongly Enhanced GFP (sGFP2). *Phys. Chem. Chem. Phys.* **2012**, *14*, 8852–8858.
(3) Gavvala, K.; Sengupta, A.; Koninti, R. K.; Hazra, P. Supramolecular Host-Inhibited Excited-State Proton Transfer and Fluorescence Switching of the Anti-Cancer Drug, Topotecan. *ChemPhysChem* **2013**, *14*, 3375–3383.
(4) Stewart, D. J.; Concepcion, J. J.; Brennaman, M. K.; Binstead, R. A.; Meyer, T. J. Accelerating Slow Excited State Proton Transfer. *Proc. Natl. Acad. Sci. U. S. A.* **2013**, *110*, 876–880.
(5) Simkovitch, R.; Shomer, S.; Gepshtein, R.; Shabat, D.; Huppert, D. Temperature Dependence of Excited-State Proton-Transfer Reaction of Quinone-Cyanine-7. *J. Phys. Chem. A* **2013**, *117*, 3925–3934.
(6) Weller, A. Fast Reactions of Excited Molecules. *Prog. React. Kinet.* **1961**, *1*, 187–214.
(7) Arnaut, L. G.; Formosinho, S. J. Excited-State Proton Transfer Reactions I. Fundamentals and Intermolecular Reactions. *J. Photochem. Photobiol., A* **1993**, *75*, 1–20.
(8) Douhal, A.; Lahmani, F.; Zewail, A. H. Proton-Transfer Reaction Dynamics. *Chem. Phys.* **1996**, *207*, 477–498.
(9) Tolbert, L. M.; Solntsev, K. M. Excited-State Proton Transfer: From Constrained Systems to "Super" Photoacids to Superfast Proton Transfer. *Acc. Chem. Res.* **2002**, *35*, 19–27.
(10) Agmon, N. Elementary Steps in Excited-State Proton Transfer. *J. Phys. Chem. A* **2005**, *109*, 13–35.
(11) Demjaschkewitch, A. B.; Zaitsev, N. K.; Kuzmin, M. G. Kinetics of Proton Transfer Reactions in the Singlet Excited State. Disproof of the Reaction from Non-Relaxed State. *Chem. Phys. Lett.* **1978**, *55*, 80–83.
(12) Tolbert, L. M.; Haubrich, J. E. Enhanced Photoacidities of Cyanonaphthols. *J. Am. Chem. Soc.* **1990**, *112*, 8163–8165.
(13) Bardez, E.; Chatelain, A.; Larrey, B.; Valeur, B. Photoinduced Coupled Proton and Electron Transfers. 1. 6-Hydroxyquinoline. *J. Phys. Chem.* **1994**, *98*, 2357–2366.
(14) Bardez, E.; Fedorov, A.; Berberan-Santos, M. N.; Martinho, J. M. G. Photoinduced Coupled Proton and Electron Transfers. 2. 7-Hydroxyquinolinium Ion. *J. Phys. Chem. A* **1999**, *103*, 4131–4136.
(15) Spry, D. B.; Goun, A.; Fayer, M. D. Deprotonation Dynamics and Stokes Shift of Pyranine (HPTS). *J. Phys. Chem. A* **2007**, *111*, 230–237.
(16) Spies, C.; Finkler, B.; Acar, N.; Jung, G. Solvatochromism of Pyranine-Derived Photoacids. *Phys. Chem. Chem. Phys.* **2013**, *15*, 19893–19905.
(17) Weller, A. Quantitative Untersuchungen der Fluoreszenzumwandlung bei Naphtholen. *Z. Elektrochem.* **1952**, *56*, 662–668.
(18) Solntsev, K. M.; Huppert, D.; Agmon, N. Solvatochromism of β-Naphthol. *J. Phys. Chem. A* **1998**, *102*, 9599–9606.
(19) Granucci, G.; Hynes, J. T.; Millié, P.; Tran-Thi, T.-H. A Theoretical Investigation of Excited-State Acidity of Phenol and Cyanophenols. *J. Am. Chem. Soc.* **2000**, *122*, 12243–12253.
(20) Agmon, N.; Rettig, W.; Groth, C. Electronic Determinants of Photoacidity in Cyanonaphtols. *J. Am. Chem. Soc.* **2002**, *124*, 1089–1096.
(21) Tolbert, L. M.; Haubrich, J. E. Photoexcited Proton Transfer from Enhanced Photoacids. *J. Am. Chem. Soc.* **1994**, *116*, 10593–10600.
(22) Smith, K. K.; Kaufmann, K. J.; Huppert, D.; Gutman, M. Picosecond Proton Ejection: An Ultrafast pH Jump. *Chem. Phys. Lett.* **1979**, *64*, 522–527.
(23) Li, Z.; Yang, Q.; Chang, R.; Ma, G.; Chen, M.; Zhang, W. N-Heteroaryl-1,8-Naphthalimide Fluorescent Sensor for Water: Molecular Design, Synthesis and Properties. *Dyes Pigm.* **2011**, *88*, 307–314.
(24) Luo, Z.; Yang, B.; Zhong, C.; Tang, F.; Yuan, M.; Xue, Y.; Yao, G.; Zhang, J.; Zhang, Y. A Dual-Channel Probe for Selective Fluoride

Determination and Application in Live Cell Imaging. *Dyes Pigm.* **2013**, *97*, 52−57.
(25) Zhu, B.; Gao, C.; Zhao, Y.; Liu, C.; Li, Y.; Wei, Q.; Ma, Z.; Du, B.; Zhang, X. A 4-Hydroxynaphthalimide-Derived Ratiometric Fluorescent Chemodosimeter for Imaging Palladium in Living Cells. *Chem. Commun.* **2011**, *47*, 8656−8658.
(26) Middleton, R. W.; Parrick, J. Preparation of 1,8-Naphthalimides as Candidate Fluorescent Probes of Hypoxic Cells. *J. Heterocycl. Chem.* **1985**, *22*, 1567−1572.
(27) Middleton, R. W.; Parrick, J.; Clarke, E. D.; Wardman, P. Synthesis and Fluorescence of N-Substituted-1,8-Naphthalimides. *J. Heterocycl. Chem.* **1986**, *23*, 849−855.
(28) Zee-Cheng, R. K. Y.; Cheng, C. C. N-(Aminoalkyl)imide Antineoplastic Agents. Synthesis and Biological Activity. *J. Med. Chem.* **1985**, *28*, 1216−1222.
(29) Biczók, L.; Valat, P.; Wintgens, V. Effect of Molecular Structure and Hydrogen Bonding on the Fluorescence of Hydroxy-Substituted Naphthalimides. *Phys. Chem. Chem. Phys.* **1999**, *1*, 4759−4766.
(30) Biczók, L.; Valat, P.; Wintgens, V. Ion Pair Formation *via* Photoinduced Proton Transfer in Excited Hydroxynaphthalimide-*N*-Methylimidazole Hydrogen Bonded Complex: Effect of Temperature and Viscosity on Dual Fluorescence. *Phys. Chem. Chem. Phys.* **2001**, *3*, 1459−1464.
(31) Biczók, L.; Valat, P.; Wintgens, V. Solvent and Temperature Effects on the Deactivation Pathways of Excited Ion Pairs Produced *via* Photoinduced Proton Transfer. *Photochem. Photobiol. Sci.* **2003**, *2*, 230−235.
(32) Eigen, M.; Kruse, W.; Maass, G.; de Maeyer, L. Rate Constants of Protolytic Reactions in Aqueous Solutions. *Prog. React. Kinet.* **1964**, *2*, 285−318.
(33) Leiderman, P.; Genosar, L.; Huppert, D. Excited-State Proton Transfer: Indication of Three Steps in the Dissociation and Recombination Process. *J. Phys. Chem. A* **2005**, *109*, 5965−5977.
(34) Krissinel, E. B.; Agmon, N. Spherical Symmetric Diffusion Problem. *J. Comput. Chem.* **1996**, *17*, 1085−1098.
(35) Förster, T.; Völker, S. Kinetics of Proton Transfer Reactions Involving Hydroxypyrene-Trisulphonate in Aqueous Solution by Nanosecond Laser Absorption Spectroscopy. *Chem. Phys. Lett.* **1975**, *34*, 1−6.
(36) Pines, E.; Huppert, D. pH Jump: A Relaxational Approach. *J. Phys. Chem.* **1983**, *87*, 4471−4478.
(37) Dziewoński, K.; Majewicz, T.; Schimmer, L. Weitere Studien über die Naphthalsäuredisubstitutionsderivate. *Bull. Int. Acad. Pol. Sci. Lett., Cl. Sci. Math. Nat., Ser. A* **1936**, 43−55.
(38) Melhuish, W. H. Quantum Efficiencies of Fluorescence of Organic Substances: Effect of Solvent and Concentration of the Fluorescent Solute. *J. Phys. Chem.* **1961**, *65*, 229−235.
(39) Brouwer, A. M. Standards for Photoluminescence Quantum Yield Measurements in Solution (IUPAC Technical Report). *Pure Appl. Chem.* **2011**, *83*, 2213−2228.
(40) *ADF2013*; SCM, Theoretical Chemistry, Vrije Universiteit: Amsterdam, The Netherlands, 2013; http://www.scm.com.
(41) te Velde, G.; Bickelhaupt, F. M.; van Gisbergen, S. J. A.; Fonseca Guerra, C.; Baerends, E. J.; Snijders, J. G.; Ziegler, T. Chemistry with ADF. *J. Comput. Chem.* **2001**, *22*, 931−967.
(42) Adamo, C.; Barone, V. Toward Reliable Density Functional Methods Without Adjustable Parameters: The PBE0 Model. *J. Chem. Phys.* **1999**, *110*, 6158−6170.
(43) Ernzerhof, M.; Scuseria, G. E. Assessment of the Perdew−Burke-Ernzerhof Exchange-Correlation Functional. *J. Chem. Phys.* **1999**, *110*, 5029−5036.
(44) van Lenthe, E.; Baerends, E. J. Optimized Slater-Type Basis Sets for the Elements 1−118. *J. Comput. Chem.* **2003**, *24*, 1142−1156.
(45) Miao, L.; Yao, Y.; Yang, F.; Wang, Z.; Li, W.; Hu, J. A TDDFT and PCM-TDDFT Studies on Absorption Spectra of N-Substituted 1,8-Naphthalimide Dyes. *J. Mol. Struct.: THEOCHEM* **2008**, *865*, 79−87.
(46) Jacquemin, D.; Perpète, E. A.; Scalmani, G.; Ciofini, I.; Peltier, C.; Adamo, C. Absorption and Emission Spectra of 1,8-Naphthalimide Fluorophores: A PCM-TD-DFT Investigation. *Chem. Phys.* **2010**, *372*, 61−66.
(47) Pye, C. C.; Ziegler, T. An Implementation of the Conductor-Like Screening Model of Solvation within the Amsterdam Density Functional Package. *Theor. Chem. Acc.* **1999**, *101*, 396−408.
(48) Förster, T. Die pH-Abhängigkeit der Fluoreszenz von Naphthalinderivaten. *Z. Elektrochem.* **1950**, *54*, 531−534.
(49) Grabowski, Z. R.; Grabowska, A. The Förster Cycle Reconsidered. *Z. Phys. Chem.* **1976**, *101*, 197−208.
(50) Fraser, R. D. B.; Suzuki, E. Resolution of Overlapping Bands: Functions for Simulating Band Shapes. *Anal. Chem.* **1969**, *41*, 37−39.
(51) Rusch, P. F.; Lelieur, J. P. Analytical Moments of Skewed Gaussian Distribution Functions. *Anal. Chem.* **1973**, *45*, 1541−1543.
(52) Blackmond, D. G. Reaction Progress Kinetic Analysis: A Powerful Methodology for Mechanistic Studies of Complex Catalytic Reactions. *Angew. Chem., Int. Ed.* **2005**, *44*, 4302−4320.
(53) Webb, S. P.; Philips, L. A.; Yeh, S. W.; Tolbert, L. M.; Clark, J. H. Picosecond Kinetics of the Excited-State, Proton-Transfer Reaction of 1-Naphthol in Water. *J. Phys. Chem.* **1986**, *90*, 5154−5164.
(54) Prémont-Schwarz, M.; Barak, T.; Pines, D.; Nibbering, E. T. J.; Pines, E. Ultrafast Excited-State Proton-Transfer Reaction of 1-Naphthol-3,6-Disulfonate and Several 5-Substituted 1-Naphthol Derivatives. *J. Phys. Chem. B* **2013**, *117*, 4594−4603.
(55) Biczók, L.; Bérces, T.; Linschitz, H. Quenching Processes in Hydrogen-Bonded Pairs: Interactions of Excited Fluorenone with Alcohols and Phenols. *J. Am. Chem. Soc.* **1997**, *119*, 11071−11077.
(56) Pines, E.; Huppert, D.; Agmon, N. Geminate Recombination in Excited-State Proton Transfer Reactions: Numerical Solution of the Debye-Smoluchowski Equation with Backreaction and Comparison with Experimental Results. *J. Chem. Phys.* **1988**, *88*, 5620−5630.
(57) Gepshtein, R.; Leiderman, P.; Genosar, L.; Huppert, D. Testing the Three Step Excited State Proton Transfer Model by the Effect of an Excess Proton. *J. Phys. Chem. A* **2005**, *109*, 9674−9684.
(58) Kumpulainen, T.; Brouwer, A. M. Excited-State Proton Transfer and Ion Pair Formation in a *Cinchona* Organocatalyst. *Phys. Chem. Chem. Phys.* **2012**, *14*, 13019−13026.
(59) Rini, M.; Magnes, B.-Z.; Pines, E.; Nibbering, E. T. J. Real-Time Observation of Bimodal Proton Transfer in Acid-Base Pairs in Water. *Science* **2003**, *301*, 349−352.
(60) Simkovitch, R.; Akulov, K.; Shomer, S.; Roth, M. E.; Shabat, D.; Schwartz, T.; Huppert, D. Comprehensive Study of Ultrafast Excited-State Proton Transfer in Water and D_2O Providing the Missing RO^- − H^+ Ion-Pair Fingerprint. *J. Phys. Chem. A* **2014**, *118*, 4425−4443.
(61) Bardez, E.; Alain, V.; Destandau, É.; Fedorov, A.; Martinho, J. M. G. Photoinduced Proton and Charge Transfers in a Dihydroxynaphthalene Derivative: Chromotropic Acid. *J. Phys. Chem. A* **2001**, *105*, 10613−10620.